Mechanics of Materials 88 (2015) 73–86

Contents lists available at ScienceDirect

Mechanics of Materials

journal homepage: www.elsevier.com/locate/mechmat

Procedures for reducing large datasets of crystal orientations using generalized spherical harmonics

Marko Knezevic *, Nicholas W. Landry

Department of Mechanical Engineering, University of New Hampshire, Durham, NH 03824, USA

ARTICLE INFO

Article history:
Received 16 February 2015
Received in revised form 22 April 2015
Available online 12 May 2015

Keywords:
Orientation distribution function
Spectral methods
Texture difference index
Anisotropy
Crystal plasticity

ABSTRACT

We present a rigorous methodology for the compaction of crystallographic texture data associated with a given material volume and show that a statistical orientation distribution function (ODF) containing any number of orientations can be compacted to a significantly smaller but representative set of orientations. This methodology is based on the spectral representation of ODFs through the use of generalized spherical harmonic functions. The Fourier coefficients of an initial full-size ODF can be matched with those of a more compact but equivalent ODF. The reduced-size ODF contains a predetermined set of representative orientations whose weights are adjusted using an algorithm for finding the closest reduced-size ODF to a given full-size ODF. To demonstrate the accuracy of the methodology, we consider three measured ODFs of two cubic metals (pure Cu and an Al alloy) and a hexagonal metal (pure Zr) and then subsequently perform plane strain and simple compression simulations with both the initial ODFs and the reduced-size ODFs. We quantitatively demonstrate that texture evolution and stress–strain response simulated with reduced-size ODFs are in excellent agreement with those simulated with initial full-size ODFs.

1. Introduction

Crystallographic texture (also called the orientation distribution function, or the ODF) is an important feature of the microstructure in polycrystalline materials known to have a strong influence on the anisotropy of various material properties (Adams and Olson, 1998; Bhattacharyya et al., 2015; Bunge, 1993; Fromm et al., 2009; Fuentes-Cobas et al., 2013; Jahedi et al., 2014; Knezevic et al., 2014a; Kocks et al., 1998). Therefore, anisotropic material models must consider the distribution of crystal orientations. In particular, modeling the anisotropy of plastic properties requires consideration of the crystal structure and orientation because of their roles in the activation of micro-scale deformation mechanisms (Taylor, 1938). A number of polycrystal plasticity material models have been developed to predict material response based on the crystallography of deformation mechanisms and the distribution of crystal orientations. These models are classified based on the homogenization scheme that links the grain scale response to the response of a polycrystalline aggregate to the mean-field models of self-consistent (Lebensohn and Tomé, 1993; Lebensohn et al., 2007) and Taylor type (Knezevic et al., 2008a; Taylor, 1938; Van Houtte et al., 2004) and the full-field models of finite-element (FE) (Kalidindi et al., 1992; Knezevic et al., 2014c; Roters et al., 2010) and Green's function fast Fourier transform (FFT) type (Lebensohn et al., 2012). Since they are physically based and able to capture the evolution of the crystallographic texture, these models are important for understanding microstructural

* Corresponding author at: Department of Mechanical Engineering, University of New Hampshire, 33 Academic Way, Kingsbury Hall, W119, Durham, NH 03824, USA. Tel.: +1 603 862 5179; fax: +1 603 862 1865.
E-mail address: marko.knezevic@unh.edu (M. Knezevic).

http://dx.doi.org/10.1016/j.mechmat.2015.04.014
0167-6636/

processes and associated effects on plasticity (Asaro and Needleman, 1985; Roters et al., 2010). As such, they are also highly desirable for performing accurate simulations of metal forming processes. Example applications include simple compression and tension tests (Beaudoin et al., 1993; Knezevic et al., 2012b), bending (Knezevic et al., 2013c,d,e), cup-drawing (Balasubramanian, 1996; Raabe and Roters, 2004), sheet hydroforming (Beaudoin et al., 1994), and bulk forming (Jahedi et al., 2015a; Knezevic et al., 2014d; Kumar and Dawson, 1995; Zecevic et al., 2015b). However, performing complex metal forming process simulations with polycrystal plasticity is recognized as a vast computational challenge because of the need for (1) specialized Newton–Raphson iterative schemes to solve sets of highly non-linear, extremely stiff constitutive equations with poor convergence characteristics for every constituent crystal at every material point and at each trial time increment and (2) storing large sets of state variables related to texture data. For example, the computational time involved in simulating a simple compression up to a strain of 0.2 with about 1000 elements and 1000 grains at an integration point is approximately 60 h on a regular PC (Knezevic et al., 2013d). Clearly, speedups are necessary to render metal forming simulations with polycrystal plasticity constructive laws practical.

From the numerical implementation point of view, several strategies have been explored to speed up the polycrystal plasticity calculations. Database approaches that store precompiled solutions in the form of spectral coefficients of the generalized spherical harmonics (GSH) basis (Kalidindi et al., 2006; Knezevic et al., 2008b; Shaffer et al., 2010; Wu et al., 2007) and the fast Fourier transform bases (Al-Harbi et al., 2010; Knezevic et al., 2009; Zecevic et al., 2015a) improved the speed for about two orders of magnitude. A process plane concept, based on proper orthogonal decomposition in Rodrigues–Frank space, has been presented in Sundararaghavan and Zabaras (2007). Other attempts to improve efficiency of the polycrystal plasticity codes rely on adaptive sampling algorithms and building a database that constantly updates itself (Barton et al., 2011, 2008). The latter methods improved the speed by about an order of magnitude. It has recently been shown that solving polycrystal plasticity using the Jacobian-Free Newton–Krylov (JFNK) technique in place of the Newton–Raphson method can yield some computational benefits (Chockalingam et al., 2013). Recently, we have successfully developed a high performance computational application of the databases approach containing discrete Fourier transforms that runs on graphic processing units (GPUs) (Mihaila et al., 2014). We have also developed an improved version that has the advantage of an efficient GPU8 algorithm for matrix–matrix multiplication (Knezevic and Savage, 2014). The latter implementation resulted in a major improvement in computational speed, exceeding three orders of magnitude over the conventional numerical schemes.

Because the computational time involved in crystal plasticity calculations scale linearly with the number of crystal orientations, the numerical schemes summarized above can further benefit from the data compaction technique aimed at minimizing the amount of state variables related to texture data. Experimental techniques for acquisition of texture data produce data sets consisting of large numbers of single crystal orientations (Jahedi et al., 2015b; Knezevic et al., 2010; Lentz et al., 2015a,b). The use of such large discrete single crystal orientations in subsequent crystal plasticity simulations is not practical, and we will show not necessary for capturing plastic anisotropy and concomitant evolution of texture. We develop a procedure for the reduction of texture data described in the form of statistical distributions (ODFs) to a level of computationally manageable but representative statistical distributions where qualitatively and quantitatively sufficient details can be recovered without losing any physical significance. The developed procedure is independent on techniques used to determine the measured full-size ODFs. The techniques for measuring ODF are broadly classified according to whether they measure macro-texture or micro-texture. The former includes X-ray diffraction (XRD) and neutron diffraction while the latter is based on electron backscattered diffraction (EBSD).

Quantitatively an ODF can be expressed by a weighted set of discrete orientations. To this end, a fundamental problem is determining a statistically significant set of discrete orientations. A number of studies for estimating the minimum number of crystal orientations representing an ODF have been conducted in the past (Baudin et al., 1995; Baudin and Penelle, 1993; Pospiech et al., 1994; Wright and Adams, 1990). The most promising methodology was based on an appropriately defined error difference between a macroscopically measured ODF and an ODF constructed from experimentally measured individual grain orientations (Baudin et al., 1995; Pospiech et al., 1994). The number of orientations in the constructed ODF was systematically increased until the error was minimized ensuring that the newly constructed ODF is statistically significant. The estimated number of orientations varied with a given ODF. Part of the reason for this variation is because weights of individual orientations were not adjusted.

The procedure developed in this paper is based on the spectral representation of ODFs using the GSH bases. A given ODF containing any number of orientations is represented by corresponding Fourier coefficients as a point in an infinite-dimensional Fourier space. We refer to this point as the target point, or the full-size target ODF. We recognize that the Fourier coefficients of the given/target full-size ODF can be matched with those of another equivalent ODF using algorithms for finding the closest reduced-size ODF to the target ODF. This key recognition led to the development of a procedure capable of reducing large datasets of crystal orientations. In our approach, the procedure starts by selecting a set of crystal orientations that cover an orientation space and delineating the complete set of all physically realizable textures using the selected orientations. The delineated space is referred to as the texture hull (Kalidindi et al., 2004; Knezevic and Kalidindi, 2007; Lyon and Adams, 2004; Wu et al., 2007) and must contain the target ODF. We then solve a linear programming problem to match the Fourier coefficients of the given ODF with those of an equivalent ODF. The methodology takes advantage of the linearity of the Fourier

space. Finally, we seek the minimum number of weighted crystal orientations in the equivalent ODF necessary for accurate modeling of the mechanical response and texture evolution. The development of these new procedures will be described in this paper.

Using this new procedure, we fitted three measured ODFs involving two cubic metals, the oxygen-free high-conductivity copper (OFHC Cu) and the magnesium–manganese–iron aluminum alloy (AA6016), and one hexagonal metal, high-purity zirconium (Zr of purity <100 ppm). These material systems were selected to demonstrate the accuracy of the procedure on distinct crystal structures, initial ODFs, and deformation mechanisms involved in plasticity. We quantitatively demonstrate that texture evolution and stress–strain response simulated with reduced-size ODFs are in excellent agreement with those simulated with the measured ODFs.

In Section 2, we describe the materials (i.e., initial texture measurements) used later in our case studies. In Section 3, we describe the fundamentals of spectral representation and the procedure in detail. In Section 4, we present the results of several case studies. Finally, the conclusions are presented in Section 5.

2. Materials

We used two face-centered cubic (FCC) metals, the oxygen-free high-conductivity copper (OFHC Cu) and the magnesium–manganese–iron aluminum alloy (AA6016), and one hexagonal close-packed (HCP) metal, Zr. Fig. 1 shows the experimental pole figures for the FCC materials. There is a noticeable difference between the initial textures of the two FCC metals. Cu has a weak texture preserved from prior rolling and AA6016 has a strong cube texture as a consequence of rolling followed by full recrystallization. Texture for the rolled and fully recrystallized AA6016 sheet was reported in Tomé et al. (2002). The initial textures for Cu and AA6016 were measured by XRD and EBSD, respectively. The Zr used in this work was the same clock rolled and annealed plate reported in Beyerlein and Tomé (2008). Fig. 2 shows a strong axisymmetric initial texture in Zr measured by EBSD. All three measured textures contained a large number of crystal orientations. The MTEX package (Bachmann et al., 2010) in MATLAB was used for plotting the pole figures in this paper.

Mechanical response was also taken from prior literature for Cu from Knezevic et al. (2014d), for AA6016 from Tomé et al. (2002), and for Zr from Beyerlein and Tomé (2008), and will be shown in the results section of the paper.

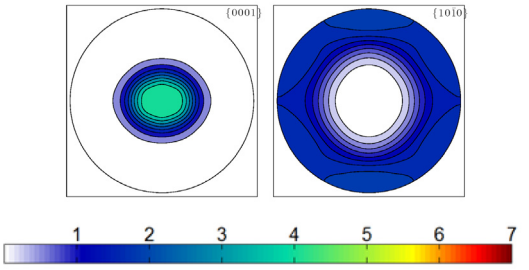

Fig. 2. Experimentally measured basal and prismatic pole figures showing initial texture for Zr.

While accommodating imposed plastic strains, grains in polycrystalline metals reorient to preferred crystallographic orientations; as a result, distribution changes. To capture the effect of texture evolution, we employ the visco-plastic self-consistent (VPSC) polycrystal plasticity model. It is this code that links the behavior of individual single crystals to that of the polycrystalline. The operating slip systems in Cu and AA6016 are $\{111\}\langle 1\bar{1}0\rangle$ Prismatic slip $\{1\bar{1}00\}\langle 11\bar{2}0\rangle$, pyramidal slip $\{10\bar{1}1\}\langle\bar{1}\bar{1}23\rangle$, and the most commonly observed twinning modes, $\{10\bar{1}2\}\langle 10\bar{1}\bar{1}\rangle$ and $\{11\bar{2}2\}\langle 11\bar{2}\bar{3}\rangle$, were considered as operative deformation mechanisms in Zr. VPSC is developed to treat these and other physical processes within single crystals (i.e., multiple slip modes, twinning modes, dislocation density evolution (Ardeljan et al., 2014; Beyerlein and Tomé, 2008; Knezevic et al., 2013b, 2012a, 2014b, 2013e), twin nucleation (Beyerlein et al., 2011b; Niezgoda et al., 2014), twin reorientation (Beyerlein et al., 2011a, 2007; Proust et al., 2007), secondary twinning (Knezevic et al., 2015) and detwinning (Knezevic et al., 2013a; Proust et al., 2010, 2009).) Within VPSC, there are also multiple options for hardening, including thermally activated dislocation density laws (Beyerlein et al., 2011b; Knezevic et al., 2014e) and the phenomenological Voce hardening law (Tomé et al., 1984). We elected to use the Voce law for FCC metals and the dislocation density law for Zr. The hardening parameters to predict stress–strain response and texture evolution were taken from Knezevic et al. (2014d) for Cu, from Tomé et al. (2002) for AA6016, and from Beyerlein and Tomé (2008) for Zr.

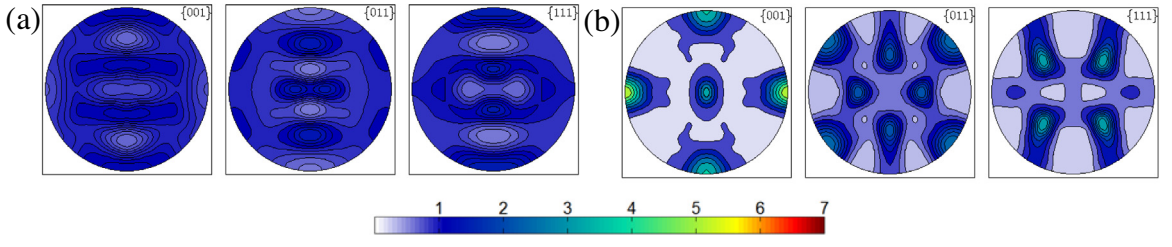

Fig. 1. Experimentally measured pole figures showing initial texture for (a) OFHC Cu and (b) AA6016.

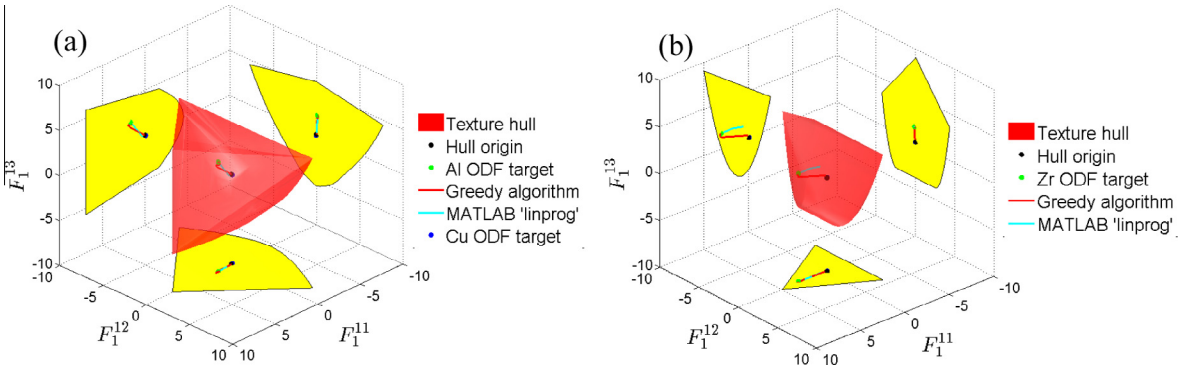

Fig. 3. Texture hull in the first three dimensions of the Fourier space for (a) cubic and (b) hexagonal materials. Each point in these convex and compact hulls represents a distinct ODF. Initial ODFs for the Al, Cu, and Zr and the fitting paths for the Al and Zr ODFs are shown in the respected hulls. The algorithms used in this work successfully fit the targeted initial ODFs.

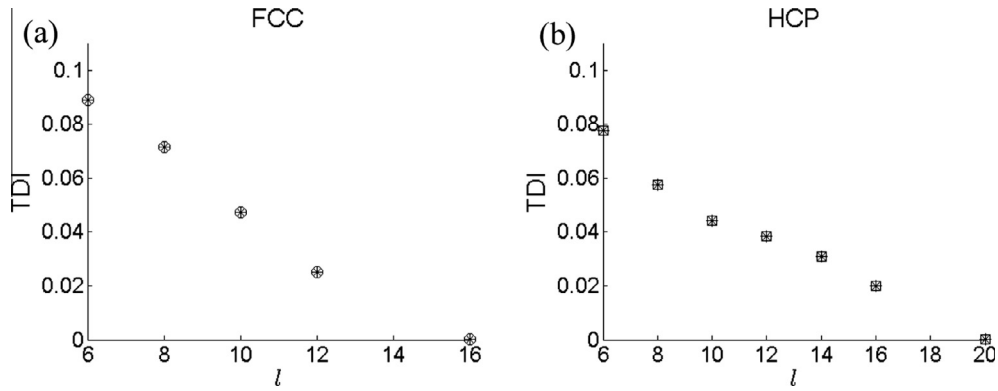

Fig. 4. Accuracy of an ODF representation defined by the texture difference index (TDI) as a function of the number of dimensions used for the representation to a large number of dimensions defined by l for (a) cubic and (b) hexagonal structure. TDI is calculated as the difference between the initial ODFs represented using $l = 16$ for FCC and $l = 20$ for HCP and the same ODFs represented using a given l.

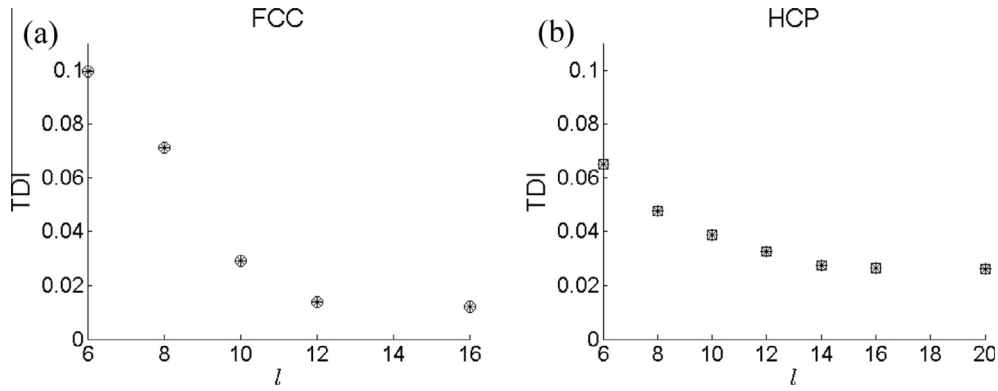

Fig. 5. TDI calculated as the difference between the initial full-size ODF and reduced-size ODFs after deformation in rolling to a strain of 0.5 for (a) cubic and (b) hexagonal materials.

3. Computational procedures for compaction of crystallographic texture

In this section, we present fundamentals of spectral representation, algorithms for finding the closest reduced-size ODF to a target ODF that is within the range of a reduced-size ODF defined by a predetermined set of crystal orientations, and quantitative measures for texture differences. The methodology for data compaction of the statistical texture data is to transform the crystal orientations of the experimental texture and a reduced-size, judiciously chosen texture data set into the Fourier space as coefficients of a series involving a GSH basis. The importance of this series representation is that the linearity of

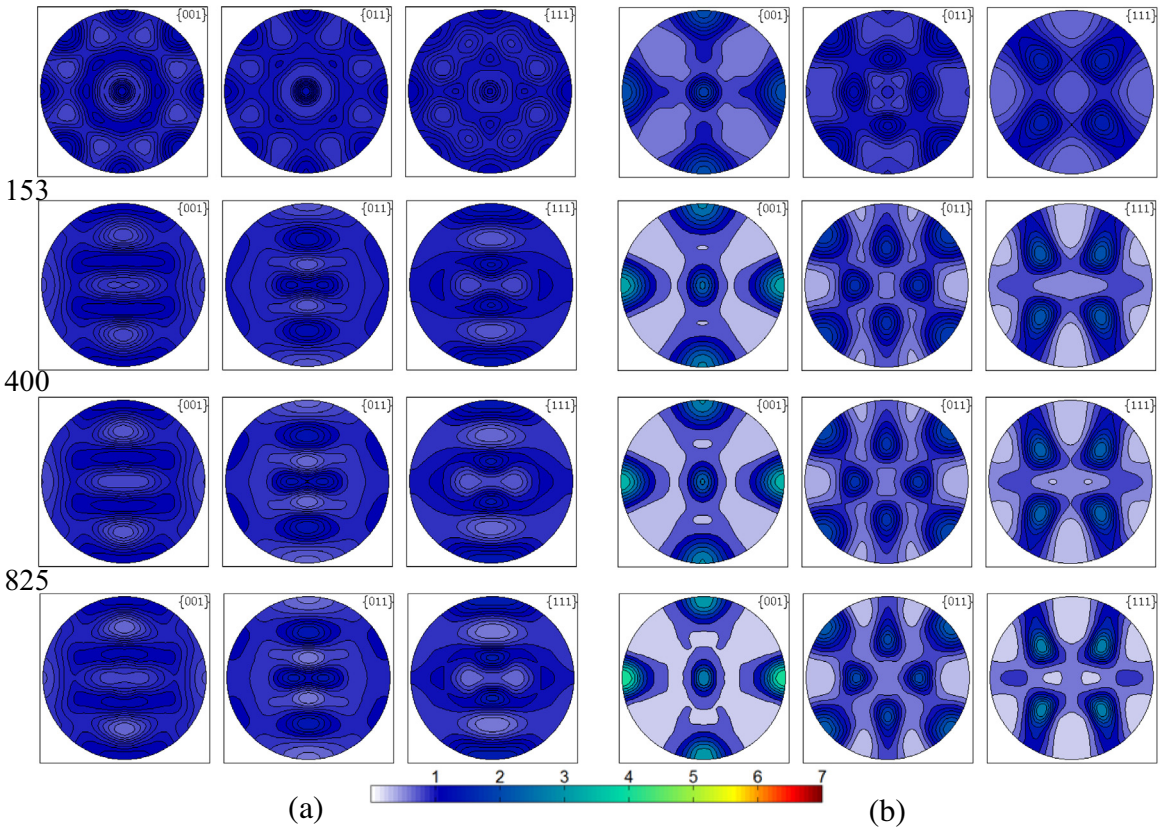

Fig. 6. Pole figures showing the reduced ODFs represented with 36, 153, 400, and 825 weighted orientations for (a) OFHC Cu and (b) AA6016.

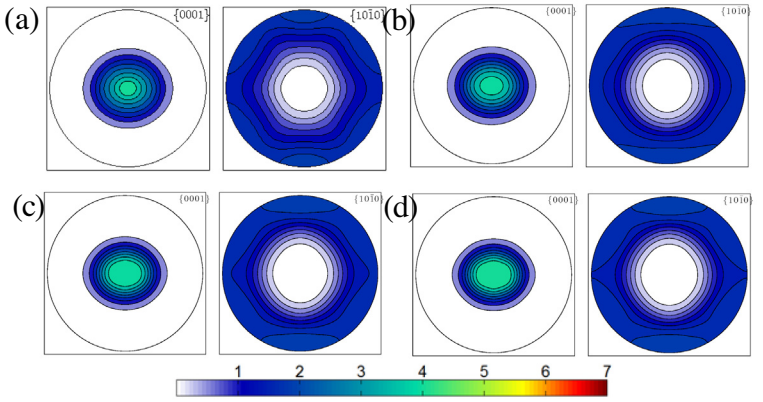

Fig. 7. Pole figures showing the reduced ODFs represented with (a) 128, (b) 432, (c) 1024, and (d) 1600 weighted orientations for Zr.

the basis can be exploited to construct a linear combination of a compact set of representative orientations to model the experimental texture.

3.1. Representation of ODF using the GSH functions

ODF, $f(g)$, is the normalized probability density associated with the occurrence of the crystallographic orientation, g, in the sample. It can be mathematically expressed as:

$$\frac{dV}{V} = f(g)dg, \quad \int_{FZ} f(g)dg = 1 \tag{1}$$

where V denotes the total sample volume and dV is the sum of all sub-volume elements in the sample associated with a lattice orientation lying within an incremental invariant volume, dg, of a given orientation, g. The FZ refers to a fundamental zone of an orientation space containing the complete set of physically distinct orientations that can occur

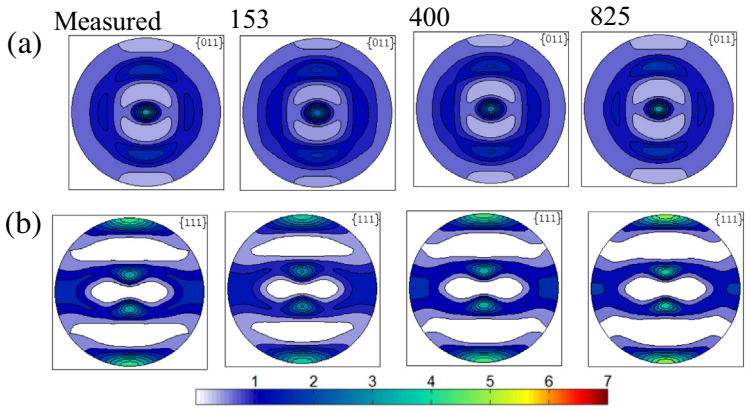

Fig. 8. Pole figures showing predicted texture for Cu after (a) simple compression (SC) to a strain of 0.25 and (b) rolling to a strain of 0.25. The simulations were performed using the measured initial texture and the reduced initial textures represented with 153, 400, and 825 weighted orientations.

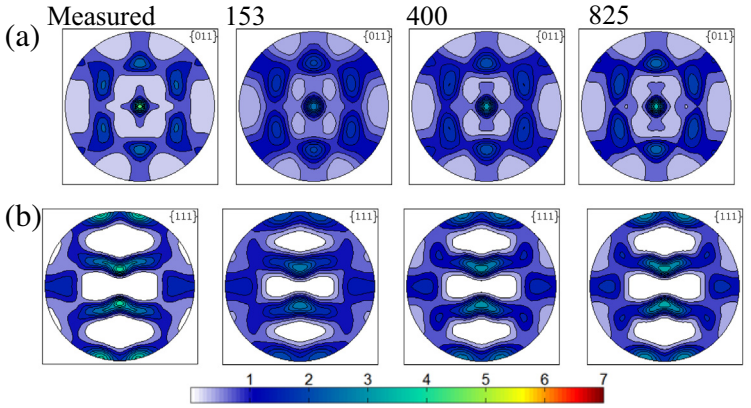

Fig. 9. Pole figures showing predicted texture for AA6016 after (a) simple compression to a strain of 0.5 (SC) and (b) rolling to a strain of 0.5. The simulations were performed using the measured initial texture and the reduced initial textures represented with 153, 400, and 825 weighted orientations.

in the sample (Bunge, 1993; Kalidindi et al., 2009). The orientation, g, can be described using any of the established representations, including a matrix of direction cosines, a set of Euler angles (Bunge, 1993), an angle-axis pair (Frank, 1987), a Rodriguez vector (Neumann, 1991), and a set of quaternions (Takahashi et al., 1985). These representations are equivalent and require the specification of three independent parameters to describe a given crystal orientation. Consequently, the orientation space of interest reduces to a three-dimensional space. In this work, we used the Bunge-Euler space for the orientation space and the Bunge-Euler angles to describe given crystal orientations. The crystal orientation is an ordered set of three rotation angles that transform the crystal local frame to the sample reference frame, i.e., $g = (\varphi_1, \Phi, \varphi_2)$. The main advantage of the Bunge–Euler space is that the rotation angles are inherently periodic.

Any ODF can be expressed efficiently in a Fourier series using GSH functions (Bunge, 1993) as:

$$f(g) = \sum_{l=0}^{\infty} \sum_{\mu=1}^{M(l)} \sum_{\nu=1}^{N(l)} F_l^{\mu\nu} T_l^{\mu\nu}(g) \tag{2}$$

where $T_l^{\mu\nu}(g)$ denotes the GSH functions and $F_l^{\mu\nu}$ are Fourier coefficients uniquely representing the ODF. The GSH are known to be the most compact Fourier basis requiring the least number of Fourier coefficients for describing ODF and the dependence of various material properties on ODF (Fuentes-Cobas et al., 2013; Kalidindi et al., 2009; Knezevic and Kalidindi, 2007) because they can be symmetrized to reflect various crystal and sample symmetries. The adopted notations for the symmetrized GSH functions are $\dot{T}_l^{\mu n}(g)$ for cubic, $\ddot{T}_l^{\mu\nu}(g)$ for cubic-orthorhombic,[1] $\dot{T}_l^{\mu n}(g)$ for hexagonal, and $\ddot{T}_l^{\mu\nu}(g)$ for hexagonal-orthorhombic crystals (Bunge, 1993). The limits $M(l)$ and $N(l)$ respectively depend on selected crystal and sample symmetry (Bunge, 1993). These limits define the number of dimensions considered for the representation of an ODF in an infinite dimensional Fourier space. We will consider the following l values for cubic metals, $l = 6$, 8, 10, 12, and 16 and $l = 6$, 8, 10, 12, 14, 16, and 20 for hexagonal metals. The correspond-

[1] The first symmetry refers to symmetry at the crystal level, while the second refers to symmetry at the sample scale.

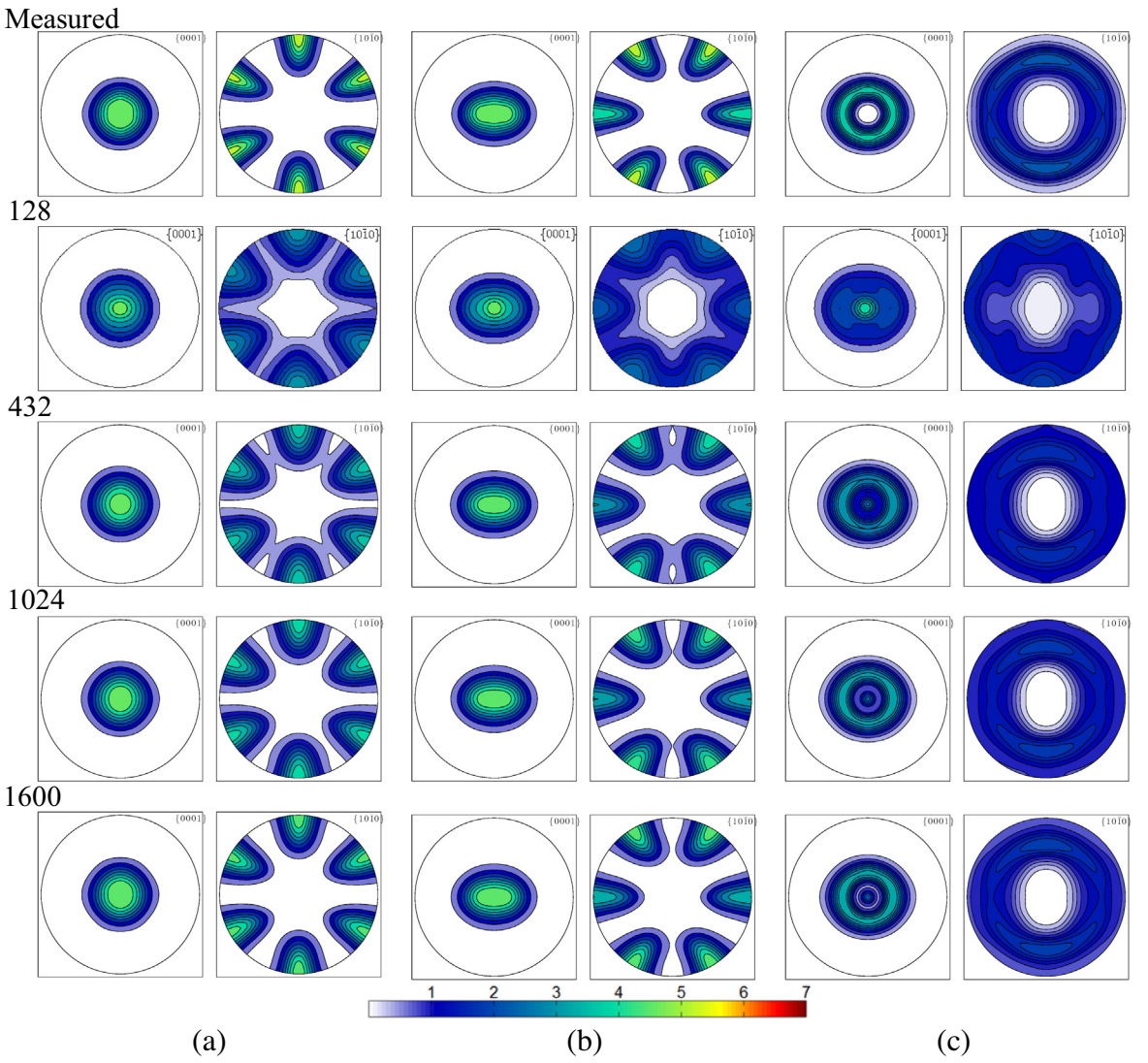

Fig. 10. Pole figures showing predicted texture of Zr deformed at 450 K to a strain of 0.3 in (a) in-plane compression (IPC), (b) in-plane tension (IPT) and (c) through-thickness compression (TTC). The simulations were performed using the measured initial texture and the reduced initial textures represented with 128, 432, 1024, and 1600 weighted orientations.

ing numbers of non-zero frequency dimensions in the Fourier space are 7, 12, 22, 36, and 75 for cubic and 14, 27, 43, 69, 105, 146, and 273 for hexagonal metals. The Fourier coefficients beyond these prescribed thresholds vanish. Typically used values of l in literature are about 10 or 12 (Knezevic and Kalidindi, 2007). The less symmetric (HCP) crystal structure demands a higher dimensional Fourier space than the more symmetric cubic crystal (Bunge, 1993; Fast et al., 2008). Eq. (2) allows visualization of ODF as a single point in an infinite dimensional Fourier space with coordinates given by $\bar{F}_l^{\mu\nu}$. If we define ${}^kF_l^{\mu\nu}$ as the Fourier coefficients of a single crystal, k, it is then possible to define a convex and compact texture hull representing the complete set of all physically realizable ODFs (Adams et al., 2001), M, as:

$$M = \left\{ F_l^{\mu\nu} \middle| \bar{F}_l^{\mu\nu} = \sum_k \alpha_k {}^kF_l^{\mu\nu}, {}^kF_l^{\mu\nu} \in M^k, \alpha_k \geq 0, \sum_k \alpha_k = 1 \right\} \quad (3)$$

where:

$$M^k = \left\{ {}^kF_l^{\mu\nu} \middle| {}^kF_l^{\mu\nu} = \frac{1}{(2l+1)} T_l^{\mu\nu'}(g^k),\ g^k \in FZ \right\} \quad (4)$$

The prime symbol (′) in the superscript of the GSH function in Eq. (4) denotes the complex conjugate. The bar on top of the Fourier coefficients in Eq. (3) indicates an averaged value of the Fourier coefficients based on the weights of crystal orientations in a given ODF.

The hulls for cubic–orthorhombic and hexagonal–orthorhombic textures are shown in the first three dimensions of the Fourier subspace in Fig. 3a and b, respectively. Note that any physically realizable texture has to have a representation inside the corresponding hull. Fig. 3a and b also depict points corresponding to the measured textures shown in Figs. 1 and 2. These measured textures are used as the full-size target textures for which, new representa-

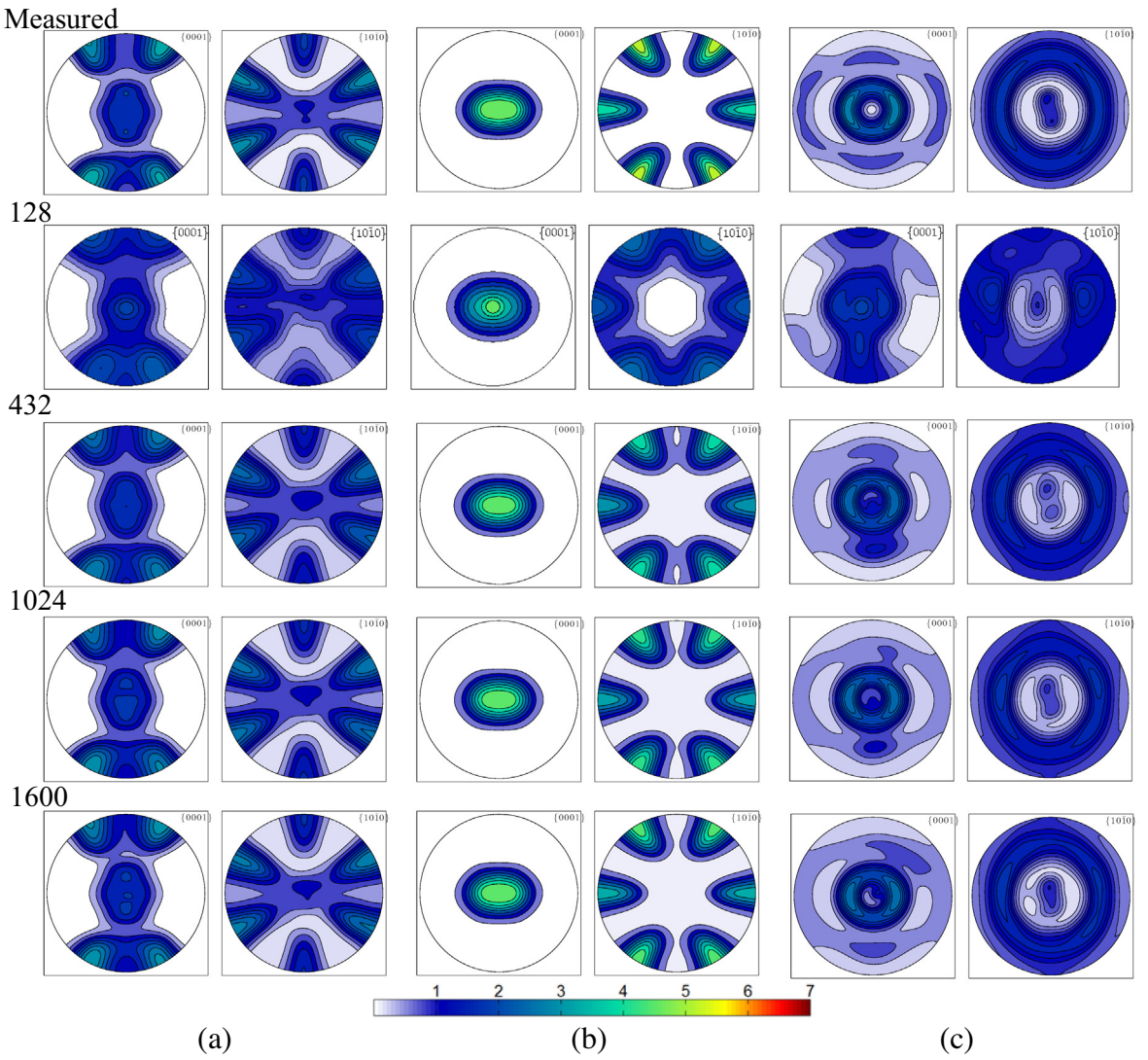

Fig. 11. Pole figures showing predicted texture of Zr deformed at 76 K to a strain of 0.3 in (a) in-plane compression (IPC), (b) in-plane tension (IPT) and (c) through-thickness compression (TTC). The simulations were performed using the measured initial texture and the reduced initial textures represented with 128, 432, 1024, and 1600 weighted orientations.

tions using reduced-size textures are sought using algorithms described in the next section.

3.2. Algorithm for finding the closest reduced-size ODF to a target full-size ODF

An ODF function is a point in an infinitely dimensional Fourier space, defined by the average value of the Fourier coefficients. Fig. 3 depicts several of such points corresponding to the measured ODFs for Cu, AA6016, and Zr. We will call these points the *target* points. We demonstrate that any target point can be fitted in the Fourier space by a significantly smaller set of weighted crystallographic orientations. The task at hand is to develop a procedure for finding the closest reduced-size ODF defined by a predetermined set of orientations to a target full-size ODF by adjusting the weights of predetermined orientations. By definition, an equivalent ODF to a given ODF is the ODF whose Fourier coefficients are identical to those of the given ODF to a prescribed value of l and a tolerance. The reduced-size ODFs contain a small number of representative orientations whose weights are adjusted during the finding process. We will call these small sets of orientations the sets of *master* orientations.

3.2.1. Binning of FZs for establishing sets of master orientations

The sets of master orientations are selected from an appropriate *FZ*. The *FZ* is discretized into bins with the constraint that each bin must have equal probability. The equal probability bins or equal volume bins are created by enforcing the invariant volume integrals to each bin using

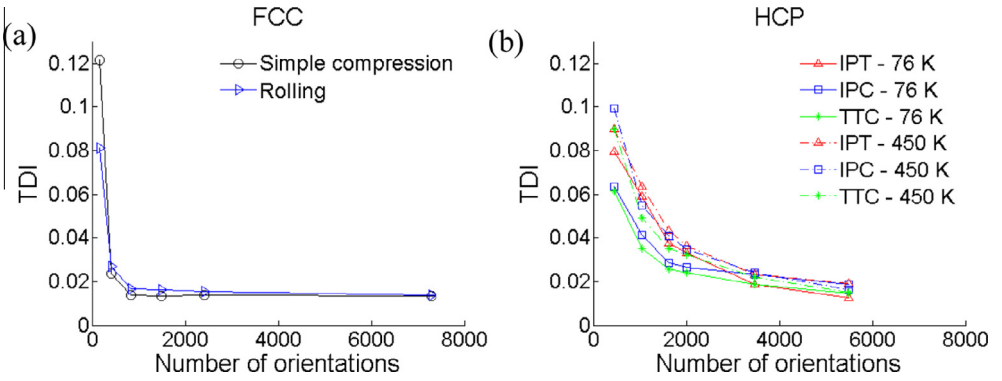

Fig. 12. Difference in the deformed textures simulated using the measured initial texture and the reduced-size initial textures represented (a) using 153, 400, 825, 1476, 2401, and 7300 weighted orientations for FCC and (b) using 432, 1024, 1600, 2000, 3456, and 5488 for HCP. Fittings of the initial ODFs were carried out using the GSH representation with $l = 12$ for FCC and $l = 14$ for HCP.

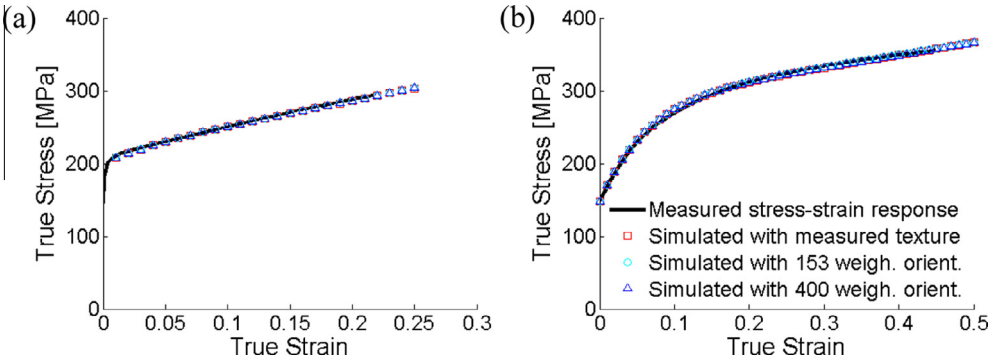

Fig. 13. Measured and simulated stress–strain responses in compression for (a) OFHC Cu and (b) AA6016. Simulations were performed using measured initial ODF and reduced initial ODFs as indicated in the figure.

$dV = \int_{\Delta\Omega} dg = \int_{\Delta\varphi_2} \int_{\Delta\Phi} \int_{\Delta\varphi_1} sin\Phi \; d\varphi_1 d\Phi d\varphi_2$. The $sin\Phi$ term accounts for the non-linearity of the Bunge-Euler space when calculating the probability of each bin. The binning procedure starts by dividing the φ_2 direction of the *FZs* by specifying a number of divisions, *N*. Next, iterations are performed to enforce equal areas, or $dA = \int_{\Delta\varphi_2} \int_{\Phi} sin\Phi \; d\Phi d\varphi_2$, in the (φ_2, Φ) plane. Subsequently, we divide the Φ direction by specifying a number of divisions, *M*. Again, the areas, $dA = \int_{\Delta\varphi_2} \int_{\Delta\Phi} sin\Phi \; d\Phi d\varphi_2$, in the (φ_2, Φ) plane are iteratively enforced to be equal. Finally, the φ_1 direction is divided by specifying a number of divisions, *L*. In this case, no iterations were required because there is no distortion of the Bunge-Euler space in the φ_1 direction. The values of N, M, and L define the coarseness of the mesh over the FZ and therefore define the number of master orientations in the sets. There are many choices to select an orientation per given bin. Moreover, the adopted binning scheme results in elongated bins in the Φ direction. The effect of equivolume binning in a five dimensional grain boundary space and associated angular distance between orientations in a given bin on grain boundary distributions has recently been studied in Glowinski and Morawiec (2014). A more sophisticated approach for selection of orientations based on the kernel density estimation technique over the binning-based method (Saylor et al., 2003) was found to substantially decrease the inherent error in computed distributions caused by equivolume binning (Glowinski and Morawiec, 2014). Here, the desired level of data compaction was achieved by simply selecting the master orientations to be corners of the invariant volume bins. The resulting ODF of master orientations with equal weights is conveniently random. Future work will explore more sophisticated ways for the selection of the master sets, which could potentially result with even greater compaction.

Because of the periodic nature of the GSH base functions, the discretization of each angle further followed the theory behind the Nyquist sampling theorem (Vaidyanathan, 2001). The Nyquist sampling criterion states that a discretization of a given function has to be finer than the frequency of a selected base function. Therefore, to robustly represent every unique linear combination of the Fourier coefficients within the convex hulls previously described, the added consideration for the binning scheme was the frequency associated with the GSH functions. For the discretization of the HCP FZ, a heuristic approach was employed to eliminate redundancies for the most compact master sets. The heuristic varied the

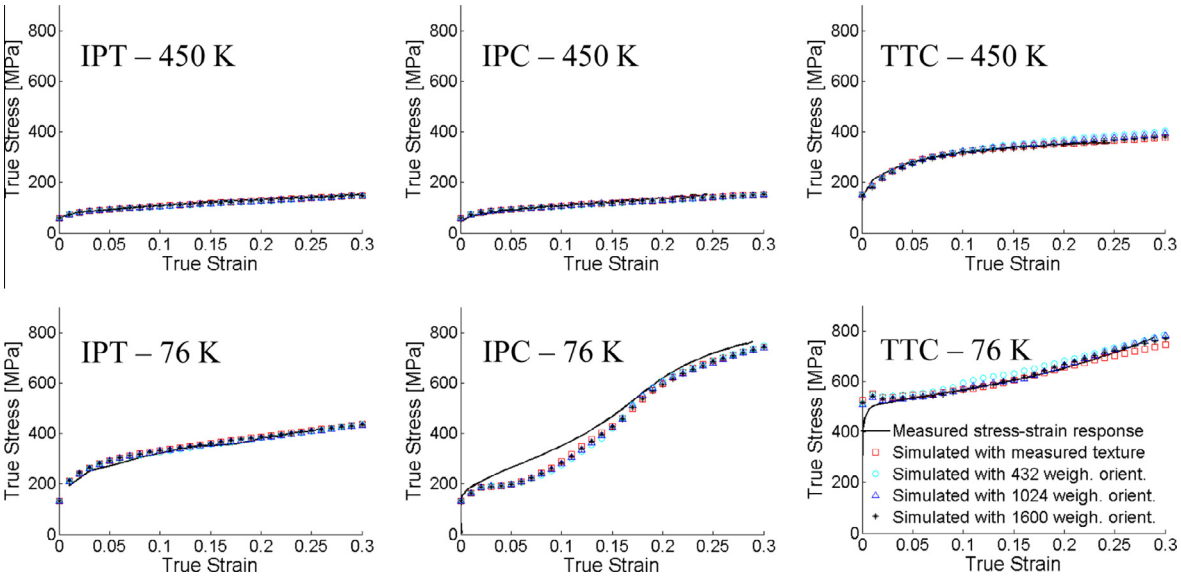

Fig. 14. Measured and simulated stress–strain responses of Zr at two temperatures, 450 and 76 K, for in-plane tension (IPT), in-plane compression (IPC), and through-thickness compression (TTC). Simulations were performed using measured initial ODF and reduced initial ODFs as indicated in the figure.

bin aspect ratios in each direction to estimate the GSH frequency while enforcing the invariant volume.

The established sets of master orientations contained N_{crys} = 36, 153, 400, 825, 1476, 2401, and 7300 orientations for cubic metals and N_{crys} = 128, 432, 1024, 1600, 2000, 3456, and 5488 orientations for HCP metals. After appropriate weight assignment to each master orientation, these sets become reduced-size ODFs. If crystal orientations in these sets are of equal weight, the resulting ODFs are random. The Fourier coefficients of the random ODFs are in the origin of the hull (see Fig. 3). Any deviation of equal weighting of master orientations in the sets results in a non-random ODF and a shift from the hull origin.

In closing this section, we reflect on the following. The convex microstructure hull contains all physically realizable textures, and theoretically, the orientation set that will provide the most efficient texture reconstruction is one that is comprised of crystal orientations with Fourier coefficients that form the boundary for this convex region up to the desired number of dimensions. These orientations were termed as the principle orientations in our previous work (Fast et al., 2008). In this earlier work, the Fourier coefficients corresponding to these principle orientations are used to calculate elastic and yield stress properties that are subsequently utilized in design and optimization of structural components made of polycrystals. However, establishing a set of principle orientations corresponding to the vertices of the hull was only possible up to a certain number of dimensions. The number of necessary dimensions in a truncation of Fourier series is dictated by the material property in consideration. As an example, only four dimensional Fourier space for FCC and nine dimensional Fourier space for HCP are necessary for calculation of elastic properties. The main challenge encountered in using the concept of principle orientations in the present work is finding the vertices of the texture hull in fairly large dimensional Fourier spaces. A more sophisticated methodology for finding these vertices in many dimensions will be sought in future works.

Next, we describe two procedures for obtaining reduced-size ODFs. The goal of these procedures is to match the average Fourier coefficients of a given target ODF and a linear combination of Fourier coefficients corresponding to master orientations.

3.2.2. Linear programming procedures for finding the closest reduced-size ODF defined by sets of master orientations to a target full-size ODF

Calculation of a reduced-size ODF is a linear programing problem that finds the closest point to a target point using a linear combination of available points in a multi-dimensional space. The target point corresponds to Fourier coefficients of the target full-size ODF and the closest point is the weighted average of Fourier coefficients of the reduced-size ODF. A solution is available as long as the target point is within the hull of the reduced-size ODF defined by a master set of orientations. In our calculations, we considered l = 6, 8, 10, 12, and 16 with the corresponding 7, 12, 22, 36, and 75 numbers of dimensions in the Fourier space for FCC and l = 6, 8, 10, 12, 14, 16, and 20 with the corresponding 14, 27, 43, 69, 105, 146, and 273 number of dimensions in the Fourier space for HCP. The number of dimensions used in the procedure influences the accuracy of representation and computational time involved in the procedure. The more dimensions used imply more accurate representations and longer computational times.

The equation and constraints to find the probability distribution of master orientations matching an initial ODF in Fourier space are:

$$F_l^{*\mu v} = {}^k\alpha {}^kF_l^{\mu v}, \quad \sum_k^{N_{crys}} {}^k\alpha = 1, 0 \le {}^k\alpha \le 1 \tag{5}$$

In Eq. (5), ${}^kF_l^{\mu v}$, are Fourier coefficients of individual orientations in a master set. We employ two different linear programming procedures aimed at establishing weights, ${}^k\alpha$, of the individual master orientations. We implement a so-called greedy algorithm and use a MATLAB "linprog" function (Matlab, 2013) to solve the linear programming problems. The greedy algorithm minimizes a distance between the target point, $F_l^{*\mu v}$, (a given full-size ODF) and the current point, $\bar{F}_l^{\mu v}$, (a reduced-size ODF):

$$d = \sqrt{\sum_l \sum_\mu \sum_v \left(F_l^{*\mu v} - (1 - {}^k\alpha)\bar{F}_l^{\mu v} - {}^k\alpha {}^kF_l^{\mu v}\right)^2} \tag{6}$$

The algorithm starts from a point in the hull corresponding to an average value of Fourier coefficients over master orientations in a given set, $\bar{F}_l^{\mu v}$. All crystals in the set have equal weight, α. Next, the algorithm searches for a crystal from the same set, ${}^kF_l^{\mu v}$, that minimizes the distance, d. Finally ${}^k\alpha$ is calculated based on the following condition $0 = \partial d/\partial\alpha$ and updated ensuring $\sum_k^{N_{crys}} {}^k\alpha = 1, 0 \le {}^k\alpha \le 1$, where k goes from 1 to the specific number of master orientations in the set. The algorithm stops when d becomes less than 10^{-8}. The MATLAB "linprog" function is based on the interior point method, and the system of equations is modified to accommodate this solver. The system of equations is reformulated using equality constraints,

$$ {}^k\alpha {}^kF_l^{\mu v} - F_l^{*\mu v} - P_l^{\mu v} + Q_l^{\mu v} = 0, \quad \sum_k^{N_{crys}} {}^k\alpha = 1 \tag{7}$$

inequality constrains,

$$ {}^k\alpha \ge 0, \quad {}^k\alpha \le 1, \quad P_l^{\mu v} \ge 0, \quad Q_l^{\mu v} \ge 0 \tag{8}$$

and the objective function for minimization,

$$\sum_l \sum_\mu \sum_v \left(P_l^{\mu v} + Q_l^{\mu v}\right) \tag{9}$$

In this formulation, $P_l^{\mu v}$ and $Q_l^{\mu v}$ are slack variables. The slack variables are utilized because they allow the linear system to become an equality constraint. These slack variables are bounded so that they cannot stay "hidden" when minimizing their sum. They are always positive and guaranteed by the bounds; however, in the equality constraint, addition and subtraction means that there is more flexibility when arriving at a solution.

Fig. 3a and b show the fitting paths for FCC and for HCP, respectively obtained by the two algorithms. Although the paths differ because the algorithms are different, the resulting ODFs and pole figures are indistinguishable. The MATLAB 'linprog' function is recommended to be used as the first choice because it is substantially faster than the greedy algorithm. It usually finds a solution is several seconds. In cases where it is unable to find a solution, we employ the slower but stable greedy algorithm. In the next section, we introduce a new measure termed here as the texture difference index (TDI) to quantify the errors involved.

3.3. Quantitative texture difference index

In order to quantify the accuracy of the spectral representation as a function of the dimensions in an infinite Fourier space, we have defined an appropriate normalized error metric expressed as:

$$\mathrm{TDI} = \frac{\sqrt{\int_{FZ} \left(f^*(g) - \bar{f}(g)\right)^2 dg}}{\sqrt{\int_{FZ} \left(f^*(g) - \tilde{f}(g)\right)^2 dg}} = \frac{\sqrt{\sum_l \sum_\mu \sum_v \left(F_l^{*\mu v} - \bar{F}_l^{\mu v}\right)^2}}{\sqrt{\sum_l \sum_\mu \sum_v \left(F_l^{*\mu v} - \tilde{F}_l^{\mu v}\right)^2}} \tag{10}$$

We call this metric the texture difference index (TDI). In Eq. (10), $f^*(g)$ denotes a given target ODF of interest typically measured using diffraction or EBSD techniques and $\bar{f}(g)$ represents the reduced-size ODF using the procedure described in the previous section. The normalization factor has been selected to represent the largest distance in the hull from $f^*(g)$. The furthest ODF and the corresponding Fourier coefficient are denoted as $\tilde{f}(g)$ and $\tilde{F}_l^{\mu v}$, respectively. This ODF is typically a single crystal. While other error definitions can be defined (Baudin et al., 1995; Pospiech et al., 1994), the adopted definition here is convenient because a TDI value of zero indicates identical ODFs, while a value of one indicates maximum theoretical disagreement between two ODFs. Note also that $\int_{FZ} f^*(g)dg = \int_{FZ} \tilde{f}(g)dg = \int_{FZ} \bar{f}(g)dg = 1$.

Fig. 4a and b depict the TDI values as a function of l for a given ODF for FCC and HCP, respectively. The values were calculated as the difference between the initial ODFs represented using $l = 16$ for FCC, $l = 20$ for HCP, and the same ODFs represented using a given l. The accuracy of the representation improves with the number of dimensions considered in an infinite Fourier space.

Fig. 5 illustrates the variation of the TDI with l for deformed textures in rolling for FCC and HCP. It can be seen that the values saturate at $l = 12$ for FCC and $l = 14$ for HCP. In other words, taking into account more dimensions will slightly improve the accuracy at the expense of computational cost. To balance accuracy with the computational efficiency of our finding the closest point code, we chose $l = 12$ for FCC and $l = 14$ for HCP. Based on Fig. 4, the level of error of the reduced-size initial texture is less than 3%.

We will use the TDI as a metric to seek the minimum number of crystallographic orientations necessary for accurate modeling of the texture evolution and the mechanical response in the case studies presented in the next section. Calculations of TDI were performed exclusively, with $l = 16$ for FCC and $l = 20$ for HCP.

4. Results and discussion

We present several case studies carefully designed to validate the procedures described in previous sections. We study two distinct crystal structures, including two FCC metals, pure Cu and AA6016 alloy, and an HCP metal, Zr. The studied FCC metals have different starting textures and exhibit different mechanical responses. While the FCC

metals deform with one slip mode, the HCP Zr deforms by multiple slip and twinning modes. To isolate deformation of Zr by multiple slip models, the simulations were performed at an elevated temperature. These conditions suppress deformation twinning and promote deformation by slip. In the most complicated case, we simulated deformation of Zr at a liquid nitrogen temperature. These conditions promote deformation twinning. We first compared the reduced-size initial ODFs with the experimental ODFs. Next, we compared texture evolution predictions at various strain levels and under different loading conditions simulated using the reduced-size ODFs and the measured full-size ODFs. Finally, we compared predictions of the anisotropic stress–strain responses simulated with the reduced-size ODFs and the measured full-size ODFs.

Fig. 6 compares results of the procedure applied to the two initial FCC textures shown in Fig. 1. The fitting was performed using sets of 36, 153, 400, and 800 master orientations. It can be seen that the set of 36 master orientations does not accurately capture features of the initial target ODFs and therefore will not be considered further. However, the set of 153 master orientations accurately qualitatively reproduce features of the initial ODFs. Similarly, Fig. 7 compares pole figures of the measured and reduced-size textures for HCP Zr. It can be seen that even the smallest set of 128 weighted master orientations qualitatively reproduce the measured texture well.

As a next test for the developed procedures, we simulate texture evolution for Cu and AA6016 in rolling and simple compression using VPSC. Figs. 8 and 9 show the predicted textures via the most relevant {011} pole for simple compression and {111} pole for rolling for both Cu and AA6016 deformed to strain levels of 0.25 and 0.5, respectively. Qualitatively, it can be seen that all the features in the pole figures obtained with the measured textures are captured with the set of 153 weighted master orientations. Figs. 10 and 11 show the predicted basal and prismatic pole figures for Zr. The initial measured texture and the corresponding reduced-size textures were deformed in compression along the in-plane (IPC) and through-thickness (TTC) directions and in tension along the in-plane direction at 450 K and 76 K to a strain of 0.3. While deformation at 450 K is mainly accommodated by slip, the deformation at 76 K is dominated by twinning, especially in IPC. Qualitatively, the results indicated that the representation with the set of 432 master orientations captures texture evolution well. Therefore, we conclude that 432 weighted orientations are sufficient to represent initial texture for HCP metals deformed by slip and twinning.

Fig. 12 quantitatively shows texture differences between predicted texture evolutions using the full initial dataset and the reduced sets. It can be seen that the error between the minimum set of master orientations determined here to be 153 for cubic metals and 420 for hexagonal metals and the full data sets is very small. The plots in Fig. 12 provide flexibility in making trade-offs between accuracy and computational speed.

Finally, in Figs. 13 and 14, we compare the stress–strain curves predicted using measured initial texture and the reduced data sets. Excellent agreement can be seen. Since the cubic metals considered here deform only by slip and are more isotropic, we present a stress–strain response in compression along the normal direction of the respected sheets. For HCP Zr we present the IPC, IPT, and TTC curves at 450 K and 76 K. These tests show that a dramatic data compaction is possible using the generalized spherical harmonics without losing accuracy in the predictions of the overall mechanical response and texture evolution.

As mentioned earlier, the computing time involved in mean-field crystal plasticity codes such as the VPSC code increases linearly with the number of grains considered in simulations. Therefore, the reduction in computing time is directly proportional to the reduction in number of grains considered in a simulation. The standalone versions of polycrystal plasticity codes facilitate simulations of relatively simple monotonic deformation processes under homogeneous boundary conditions. To enables simulations of complex, non-monotonic deformation process with heterogeneous boundary conditions these codes are embedded within finite elements. The procedure developed in the present paper is primarily intended to increase efficiency of these codes. The VPSC model has recently been integrated within finite elements (Knezevic et al., 2013d). For the specific example mentioned in the introduction of the present paper that utilized the finite element VPSC implementation, the computational time involved would reduce by over six times (from 60 h to approximately 10 h) if the number of grains considered per FE integration point would drop from 1000 to 153.

5. Summary and conclusions

Microstructure based simulations of metal forming processes and microstructure sensitive designs for material performance optimization at the macro-scale are impractical in part because of the need to store many state variables associated with microstructure data. In this work, we have successfully developed procedures for the reduction of large statistical distributions of crystallographic texture data to computationally manageable distributions. The developed procedures are based on the spectral representation of texture using generalized spherical harmonic functions. Compact sets of master orientation were selected based on the Nyquist sampling theorem from the orientation space for cubic and hexagonal structures and shown sufficient for reducing any ODF by formulating a constrained linear optimization in Fourier space. Our case studies demonstrated the power of the spectral representation and the benefits of the linear Fourier space when dealing with large data sets. We accurately modeled microstructure and material response after reducing millions of crystal orientations to significantly smaller sets of weighted master orientations. The procedures were applied to both cubic and hexagonal crystal structures and shown to work well for metals deforming with both slip and twinning mechanisms. The minimum set of master orientations was determined to be 153 for cubic metals and 432 for hexagonal metals. Using these numbers of orientations, the simulated stress–strain response and texture evolution were nearly indistinguishable from those

simulated using full data sets. A new measure for quantitative ODF comparisons that takes advantage of the spectral representations was introduced. This measure was termed the texture difference index (TDI) and represents a suitable normalized distance between two ODFs in the Fourier space. Using this quantitative measure, we have shown that the error involved in simulations using the minimal sets of orientations is negligible. In addition, the methodology provided flexibility in making trade-offs between accuracy and computational speed.

The established procedures can significantly improve computational efficiency of microstructure-sensitive simulations and help effectuate microstructure informed materials design, and thus, contribute to a genesis of new material development.

Acknowledgements

This work is based upon project supported by the National Science Foundation under Grant CMMI-1301081. NWL acknowledges summer fellowship from the Hamel Center for Undergraduate Research at the University of New Hampshire (UNH). The authors also acknowledge numerous discussions with Professor Mark Lyon of UNH.

References

Adams, B.L., Olson, T., 1998. Mesostructure – properties linkage in polycrystals. Prog. Mater. Sci. 43, 1–88.
Adams, B.L., Henrie, A., Henrie, B., Lyon, M., Kalidindi, S.R., Garmestani, H., 2001. Microstructure-sensitive design of a compliant beam. J. Mech. Phys. Solids 49, 1639–1663.
Al-Harbi, H.F., Knezevic, M., Kalidindi, S.R., 2010. Spectral approaches for the fast computation of yield surfaces and first-order plastic property closures for polycrystalline materials with cubic-triclinic textures. CMC Comput. Mater. Continua 15, 153–172.
Ardeljan, M., Beyerlein, I.J., Knezevic, M., 2014. A dislocation density based crystal plasticity finite element model: application to a two-phase polycrystalline HCP/BCC composites. J. Mech. Phys. Solids 66, 16–31.
Asaro, R.J., Needleman, A., 1985. Texture development and strain hardening in rate dependent polycrystals. Acta Metall. Mater. 33, 923–953.
Bachmann, F., Hielscher, R., Schaeben, H., 2010. Texture analysis with MTEX–free and open source software toolbox. Solid State Phenom. 160, 63–68.
Balasubramanian, 1996. Single crystal and polycrystal elasto-viscoplasticity: application to earing in cup drawing of F.C.C. materials. Comput. Mech. 17, 209–225.
Barton, N.R., Knap, J., Arsenlis, A., Becker, R., Hornung, R.D., Jefferson, D.R., 2008. Embedded polycrystal plasticity and adaptive sampling. Int. J. Plast. 24, 242–266.
Barton, N., Bernier, J., Knap, J., Sunwoo, A., Cerreta, E., Turner, T., 2011. A call to arms for task parallelism in multi-scale materials modeling. Int. J. Numer. Methods Eng. 86, 744–764.
Baudin, T., Penelle, R., 1993. Determination of the total texture. MTA 24, 2299–2311.
Baudin, T., Jura, J., Penelle, R., Pospiech, J., 1995. Estimation of the minimum grain number for the orientation distribution function calculation from individual orientation Measurements on Fe–3% Si and Ti–4Al–6V alloys. J. Appl. Crystallogr. 28, 582–589.
Beaudoin, A.J., Mathur, K.K., Dawson, P.R., Johnson, G.C., 1993. Three-dimensional deformation process simulation with explicit use of polycrystal plasticity models. Int. J. Plast. 9, 833–860.
Beaudoin, A.J., Dawson, P.R., Mathur, K.K., Kocks, U.F., Korzekwa, D.A., 1994. Application of polycrystal plasticity to sheet forming. Comput. Methods Appl. Mech. Eng. 117, 49–70.
Beyerlein, I.J., Tomé, C.N., 2008. A dislocation-based constitutive law for pure Zr including temperature effects. Int. J. Plast. 24, 867–895.
Beyerlein, I.J., Tóth, L.S., Tomé, C.N., Suwas, S., 2007. Role of twinning on texture evolution of silver during equal channel angular extrusion. Philos. Mag. 87, 885–906.
Beyerlein, I.J., Mara, N.A., Bhattacharyya, D., Alexander, D.J., Necker, C.T., 2011a. Texture evolution via combined slip and deformation twinning in rolled silver–copper cast eutectic nanocomposite. Int. J. Plast. 27, 121–146.
Beyerlein, I.J., McCabe, R.J., Tomé, C.N., 2011b. Effect of microstructure on the nucleation of deformation twins in polycrystalline high-purity magnesium: a multi-scale modeling study. J. Mech. Phys. Solids 59, 988–1003.
Bhattacharyya, A., Knezevic, M., Abouaf, M., 2015. Characterization of crystallographic texture and intra-grain morphology in cross-rolled tantalum. Metall. Mater. Trans. A 46, 1085–1096.
Bunge, H.-J., 1993. Texture analysis in materials science. In: Mathematical Methods. Cuvillier Verlag, Göttingen.
Chockalingam, K., Tonks, M.R., Hales, J.D., Gaston, D.R., Millett, P.C., Zhang, L., 2013. Crystal plasticity with Jacobian-Free Newton–Krylov. Comput. Mech. 51, 617–627.
Fast, T., Knezevic, M., Kalidindi, S.R., 2008. Application of microstructure sensitive design to structural components produced from hexagonal polycrystalline metals. Comput. Mater. Sci. 43, 374–383.
Frank, F.C., 1987. Orientation mapping. MTA 19A, 403–408.
Fromm, B.S., Adams, B.L., Ahmadi, S., Knezevic, M., 2009. Grain size and orientation distributions: application to yielding of α-titanium. Acta Mater. 57, 2339–2348.
Fuentes-Cobas, L.E., Muñoz-Romero, A., Montero-Cabrera, M.E., Fuentes-Montero, L., Fuentes-Montero, M.E., 2013. Predicting the coupling properties of axially-textured materials. Materials 6, 4967–4984.
Glowinski, K., Morawiec, A., 2014. Analysis of experimental grain boundary distributions based on boundary-space metrics. Metall. Mater. Trans. A 45, 3189–3194.
Jahedi, M., Paydar, M.H., Zheng, S., Beyerlein, I.J., Knezevic, M., 2014. Texture evolution and enhanced grain refinement under high-pressure-double-torsion. Mater. Sci. Eng. A 611, 29–36.
Jahedi, M., Knezevic, M., Paydar, M., 2015a. High-pressure double torsion as a severe plastic deformation process: experimental procedure and finite element modeling. J. Mater. Eng. Perform. 24, 1471–1482.
Jahedi, M., Paydar, M.H., Knezevic, M., 2015b. Enhanced microstructural homogeneity in metal–matrix composites developed under high-pressure-double-torsion. Mater. Charact. 104, 92–100.
Kalidindi, S.R., Bronkhorst, C.A., Anand, L., 1992. Crystallographic texture evolution in bulk deformation processing of fcc metals. J. Mech. Phys. Solids 40, 537–569.
Kalidindi, S.R., Houskamp, J.R., Lyons, M., Adams, B.L., 2004. Microstructure sensitive design of an orthotropic plate subjected to tensile load. Int. J. Plast. 20, 1561–1575.
Kalidindi, S.R., Duvvuru, H.K., Knezevic, M., 2006. Spectral calibration of crystal plasticity models. Acta Mater. 54, 1795–1804.
Kalidindi, S.R., Knezevic, M., Niezgoda, S., Shaffer, J., 2009. Representation of the orientation distribution function and computation of first-order elastic properties closures using discrete Fourier transforms. Acta Mater. 57, 3916–3923.
Knezevic, M., Kalidindi, S.R., 2007. Fast computation of first-order elastic–plastic closures for polycrystalline cubic–orthorhombic microstructures. Comput. Mater. Sci. 39, 643–648.
Knezevic, M., Savage, D.J., 2014. A high-performance computational framework for fast crystal plasticity simulations. Comput. Mater. Sci. 83, 101–106.
Knezevic, M., Kalidindi, S.R., Fullwood, D., 2008a. Computationally efficient database and spectral interpolation for fully plastic Taylor-type crystal plasticity calculations of face-centered cubic polycrystals. Int. J. Plast. 24, 1264–1276.
Knezevic, M., Kalidindi, S.R., Mishra, R.K., 2008b. Delineation of first-order closures for plastic properties requiring explicit consideration of strain hardening and crystallographic texture evolution. Int. J. Plast. 24, 327–342.
Knezevic, M., Al-Harbi, H.F., Kalidindi, S.R., 2009. Crystal plasticity simulations using discrete Fourier transforms. Acta Mater. 57, 1777–1784.
Knezevic, M., Levinson, A., Harris, R., Mishra, R.K., Doherty, R.D., Kalidindi, S.R., 2010. Deformation twinning in AZ31: influence on strain hardening and texture evolution. Acta Mater. 58, 6230–6242.
Knezevic, M., Capolungo, L., Tomé, C.N., Lebensohn, R.A., Alexander, D.J., Mihaila, B., McCabe, R.J., 2012a. Anisotropic stress–strain response and microstructure evolution of textured α-uranium. Acta Mater. 60, 702–715.
Knezevic, M., McCabe, R.J., Lebensohn, R.A., Tomé, C.N., Mihaila, B., 2012b. Finite element implementation of a self-consistent polycrystal

plasticity model: application to α-uranium. In: Proceedings: Volume 2: Materials Properties, Characterization, and Modeling TMS, The Minerals, Metals & Materials Society, pp. 789–796.
Knezevic, M., Beyerlein, I.J., Brown, D.W., Sisneros, T.A., Tomé, C.N., 2013a. A polycrystal plasticity model for predicting mechanical response and texture evolution during strain-path changes: application to beryllium. Int. J. Plast. 49, 185–198.
Knezevic, M., Beyerlein, I.J., Nizolek, T., Mara, N.A., Pollock, T.M., 2013b. Anomalous basal slip activity in zirconium under high-strain deformation. Mater. Res. Lett. 1, 133–140.
Knezevic, M., Lebensohn, R.A., Cazacu, O., Revil-Baudard, B., Proust, G., Vogel, S.C., Nixon, M.E., 2013c. Modeling bending of α-titanium with embedded polycrystal plasticity in implicit finite elements. Mater. Sci. Eng. A 564, 116–126.
Knezevic, M., McCabe, R.J., Lebensohn, R.A., Tomé, C.N., Liu, C., Lovato, M.L., Mihaila, B., 2013d. Integration of self-consistent polycrystal plasticity with dislocation density based hardening laws within an implicit finite element framework: application to low-symmetry metals. J. Mech. Phys. Solids 61, 2034–2046.
Knezevic, M., McCabe, R.J., Tomé, C.N., Lebensohn, R.A., Chen, S.R., Cady, C.M., Gray Iii, G.T., Mihaila, B., 2013e. Modeling mechanical response and texture evolution of α-uranium as a function of strain rate and temperature using polycrystal plasticity. Int. J. Plast. 43, 70–84.
Knezevic, M., Beyerlein, I.J., Lovato, M.L., Tomé, C.N., Richards, A.W., McCabe, R.J., 2014a. A strain-rate and temperature dependent constitutive model for BCC metals incorporating non-Schmid effects: application to tantalum–tungsten alloys. Int. J. Plast. 62, 93–104.
Knezevic, M., Carpenter, J.S., Lovato, M.L., McCabe, R.J., 2014b. Deformation behavior of the cobalt-based superalloy Haynes 25: experimental characterization and crystal plasticity modeling. Acta Mater. 63, 162–168.
Knezevic, M., Drach, B., Ardeljan, M., Beyerlein, I.J., 2014c. Three dimensional predictions of grain scale plasticity and grain boundaries using crystal plasticity finite element models. Comput. Methods Appl. Mech. Eng. 277, 239–259.
Knezevic, M., Jahedi, M., Korkolis, Y.P., Beyerlein, I.J., 2014d. Material-based design of the extrusion of bimetallic tubes. Comput. Mater. Sci. 95, 63–73.
Knezevic, M., Nizolek, T., Ardeljan, M., Beyerlein, I.J., Mara, N.A., Pollock, T.M., 2014e. Texture evolution in two-phase Zr/Nb lamellar composites during accumulative roll bonding. Int. J. Plast. 57, 16–28.
Knezevic, M., Zecevic, M., Beyerlein, I.J., Bingert, J.F., McCabe, R.J., 2015. Strain rate and temperature effects on the selection of primary and secondary slip and twinning systems in HCP Zr. Acta Mater. 88, 55–73.
Kocks, U.F., Tome', C.N., Wenk, H.-R., 1998. Texture and Anisotropy. Cambridge University Press, Cambridge.
Kumar, A., Dawson, P., 1995. Polycrystal plasticity modeling of bulk forming with finite elements over orientation space. Comput. Mech. 17, 10–25.
Lebensohn, R.A., Tomé, C.N., 1993. A self-consistent anisotropic approach for the simulation of plastic deformation and texture development of polycrystals: application to zirconium alloys. Acta Metall. Mater. 41, 2611–2624.
Lebensohn, R.A., Tomé, C.N., Castaneda, P.P., 2007. Self-consistent modelling of the mechanical behaviour of viscoplastic polycrystals incorporating intragranular field fluctuations. Philos. Mag. 87, 4287–4322.
Lebensohn, R.A., Kanjarla, A.K., Eisenlohr, P., 2012. An elasto-viscoplastic formulation based on fast Fourier transforms for the prediction of micromechanical fields in polycrystalline materials. Int. J. Plast. 32–33, 59–69.
Lentz, M., Klaus, M., Beyerlein, I.J., Zecevic, M., Reimers, W., Knezevic, M., 2015a. In situ X-ray diffraction and crystal plasticity modeling of the deformation behavior of extruded Mg–Li–(Al) alloys: an uncommon tension–compression asymmetry. Acta Mater. 86, 254–268.
Lentz, M., Klaus, M., Wagner, M., Fahrenson, C., Beyerlein, I.J., Zecevic, M., Reimers, W., Knezevic, M., 2015b. Effect of age hardening on the deformation behavior of an Mg–Y–Nd alloy: in-situ X-ray diffraction and crystal plasticity modeling. Mater. Sci. Eng. A 628, 396–409.
Lyon, M., Adams, B.L., 2004. Gradient-based non-linear microstructure design. J. Mech. Phys. Solids 52, 2569–2586.
MATLAB Version R2012a, 2013. The MathWorks Inc., Natick, MA, USA.
Mihaila, B., Knezevic, M., Cardenas, A., 2014. Three orders of magnitude improved efficiency with high-performance spectral crystal plasticity on GPU platforms. Int. J. Numer. Methods Eng. 97, 785–798.
Neumann, P., 1991. Representation of orientations of symmetrical objects by Rodrigues vectors. Text. Microstruct. 14–18, 53–58.
Niezgoda, S.R., Kanjarla, A.K., Beyerlein, I.J., Tomé, C.N., 2014. Stochastic modeling of twin nucleation in polycrystals: an application in hexagonal close-packed metals. Int. J. Plast. 56, 119–138.
Pospiech, J., Jura, J., Gottstein, G., 1994. Statistical analysis of single grain orientation data generated from model textures. In: Materials Science Forum. Trans Tech Publ, pp. 407–412.
Proust, G., Tomé, C.N., Kaschner, G.C., 2007. Modeling texture, twinning and hardening evolution during deformation of hexagonal materials. Acta Mater. 55, 2137–2148.
Proust, G., Tomé, C.N., Jain, A., Agnew, S.R., 2009. Modeling the effect of twinning and detwinning during strain-path changes of magnesium alloy AZ31. Int. J. Plast. 25, 861–880.
Proust, G., Kaschner, G.C., Beyerlein, I.J., Clausen, B., Brown, D.W., McCabe, R.J., Tomé, C.N., 2010. Detwinning of high-purity zirconium: in-situ neutron diffraction experiments. Exp. Mech. 50, 125–133.
Raabe, D., Roters, F., 2004. Using texture components in crystal plasticity finite element simulations. Int J. Plast. 20, 339–361.
Roters, F., Eisenlohr, P., Hantcherli, L., Tjahjanto, D.D., Bieler, T.R., Raabe, D., 2010. Overview of constitutive laws, kinematics, homogenization and multiscale methods in crystal plasticity finite-element modeling: theory, experiments, applications. Acta Mater. 58, 1152–1211.
Saylor, D.M., Morawiec, A., Rohrer, G.S., 2003. Distribution of grain boundaries in magnesia as a function of five macroscopic parameters. Acta Mater. 51, 3663–3674.
Shaffer, J.B., Knezevic, M., Kalidindi, S.R., 2010. Building texture evolution networks for deformation processing of polycrystalline fcc metals using spectral approaches: applications to process design for targeted performance. Int. J. Plast. 26, 1183–1194.
Sundararaghavan, V., Zabaras, N., 2007. Linear analysis of texture-property relationships using process-based representations of Rodrigues space. Acta Mater. 55, 1573–1587.
Takahashi, Y., Miyazawa, K.I., Mori, M., Ishida, Y., 1985. Quaternion representation of the orientation relationship and its application to grain boundary problems. Trans. Jpn. Inst. Met. 27, 345–352.
Taylor, G.I., 1938. Plastic strain in metals. J. Inst. Met. 62, 307–324.
Tomé, C., Canova, G.R., Kocks, U.F., Christodoulou, N., Jonas, J.J., 1984. The relation between macroscopic and microscopic strain hardening in F.C.C. polycrystals. Acta Metall. 32, 1637–1653.
Tomé, C., Necker, C., Lebensohn, R., 2002. Mechanical anisotropy and grain interaction in recrystallized aluminum. Metall. Mater. Trans. A 33, 2635–2648.
Vaidyanathan, P., 2001. Generalizations of the sampling theorem: seven decades after Nyquist. IEEE Trans. Circuits Syst. I Fundam. Theory Appl. 48, 1094–1109.
Van Houtte, P., Li, S., Engler, O., 2004. Taylor-type homogenization methods for texture and anisotropy. In: Continuum Scale Simulation of Engineering Materials: Fundamentals-Microstructures-Process Applications. Wiley-VCH Verlag GmbH & Co. KGaA, Weinheim, pp. 459–472.
Wright, S.I., Adams, B.L., 1990. An evaluation of the single orientation method for texture determination in materials of moderate texture strength. Text. Microstruct. 12, 65–76.
Wu, X., Proust, G., Knezevic, M., Kalidindi, S.R., 2007. Elastic–plastic property closures for hexagonal close-packed polycrystalline metals using first-order bounding theories. Acta Mater. 55, 2729–2737.
Zecevic, M., McCabe, R.J., Knezevic, M., 2015a. A new implementation of the spectral crystal plasticity framework in implicit finite elements. Mech. Mater. 84, 114–126.
Zecevic, M., McCabe, R.J., Knezevic, M., 2015b. Spectral database solutions to elasto-viscoplasticity within finite elements: application to a cobalt-based FCC superalloy. Int. J. Plast. 70, 151–165.